

Adaptive Bayesian Changepoint Analysis & Local Outlier Scoring

Haoxuan Wu and David S. Matteson

Cornell University

December 22, 2024

Abstract

We introduce global-local shrinkage priors into a Bayesian dynamic linear model to adaptively estimate both changepoints and local outliers in a novel model we call Adaptive Bayesian Changepoints with Outliers (ABCO). We utilize a state-space approach to identify a dynamic signal in the presence of outliers and measurement error with stochastic volatility. We find that global state equation parameters are inadequate for most real applications and we include local parameters to track noise at each time-step. This setup provides a flexible framework to detect unspecified changepoints in complex series, such as those with large interruptions in local trends, with robustness to outliers and heteroskedastic noise. ABCO may also be used as a robust Bayesian trend filter that can reconstruct interrupted time series. We detail the extension of our approach to time-varying parameter estimation within dynamic regression analysis to identify structural breaks. Finally, we compare our algorithm against several alternatives to demonstrate its efficacy in diverse simulation scenarios and two empirical examples.¹

Keywords: Anomaly Detection; Interrupted Time Series; Stochastic Volatility; Structural Change; Trend Filtering

1 Introduction

Changepoint analysis involves detecting changes in the distribution of a time series. This field has a wide variety of applications: in genetics, it is used to identify changes within DNA sequences (Braun *et al.*, 2000); in environmental science, it is applied to quantify climate change (Solow, 1987); in finance, it helps gain insights into historical data and improves future forecasting (Chen and Gupta, 1997); in EEG analysis, it identifies key signals for monitoring health status of patients (Chen *et al.*, 2019). As these examples illustrate, modern time series is characterized by increased complexity and decreased homogeneity (Rehman *et al.*, 2016). In this article, we aim to understand how the underlying distribution

¹Financial support is gratefully acknowledged from a Xerox PARC Faculty Research Award, National Science Foundation Awards 1455172, 1934985, 1940124, and 1940276, USAID, and Cornell University Atkinson Center for a Sustainable Future.

of a time series changes, to distinguish unspecified local trends from major changes, and to do so in the presence of stochastic volatility and outliers. The flexible and adaptive framework we propose can extend the application of changepoint analysis to even more domains of research.

Many approaches have been used to identify changepoints. One approach considers the changepoint problem as anomaly detection (Aminikhanghahi and Cook, 2017). Another approach is to apply a statistic, such as cumulative sum (Cho and Fryzlewicz, 2015), energy distance (Matteson and James, 2014) or Kullback-divergence (Liu *et al.*, 2013), to segment a series into contiguous clusters. Identifying breaks within state-space models has also been proposed (Kawahara *et al.*, 2007). These approaches all focus on estimating the number and locations of changepoints, but they have limited flexibility and do not typically provide uncertainty quantification.

From the Bayesian perspective, changepoints can be considered locations that partition data into contiguous clusters generated from different probability distributions (Adams and MacKay, 2007). Recursive Bayesian inversion paired with importance sampling can be applied to analyze the probability of a sequence coming from a common probability distribution (Tan *et al.*, 2015). However, this, and many other approaches, makes the strong assumption that observations within each segment are independent and identically distributed (iid), which greatly limits the scope of suitable applications.

In related literature, one can find changepoint detection methods based on recurrent neural network (Ebrahimzadeh *et al.*, 2019), Gaussian processes (Saatçi *et al.*, 2010), and hidden Markov models (Montanez *et al.*, 2015). Such approaches can be extremely flexible, but many lack robustness or are ‘black-box’ in nature, lacking interpretability. They may also require large training series, expert structural specification, and extensive hyper-parameter selection.

Nearly all existing changepoint algorithms are unreliable in the presence of unlabeled outliers or heteroskedastic noise. Outliers substantially change distributional estimates and violate the common assumption of many algorithms of Gaussian noise. To address changepoint analysis in the presence of outliers, Fearnhead and Rigall (2017) proposed an alternative biweight loss function to cap the influence of individual observations. While successful, the algorithm is sensitive to tuning parameters for both the influence threshold and the number of change points, which are difficult to specify in practice. Giordani *et al.* (2007) proposed a state-space framework that incorporates thresholding for modeling smooth transitions and Markov switching for modeling outliers. While also successful, this method lacks robustness to heteroskedastic data, over-segmenting series in high volatility periods.

In this paper, we propose a new method called Adaptive Bayesian Changepoints with Outliers (ABCO). At its core, ABCO utilizes a threshold autoregressive stochastic volatility process within a time-varying parameter model to estimate smoothly varying trends with large, isolated interruptions. Through a state-space framework, ABCO successfully models heteroskedastic measurement error, and jointly identifies both local outliers and changepoints. Utilizing several efficient sampling techniques,

ABCO is also computationally efficient, with complexity $\mathcal{O}(\mathcal{T})$ for a length T series. Within the observation equation, we decompose a series into three basic components: a locally varying trend signal, a sparse additive outlier signal, and a heteroskedastic noise process. Our specification allows locally adaptive modeling for both trend and variability, automatically adjusting changepoint and outlier detection to periods of high and low volatility.

ABCO’s trend modeling greatly extends the Bayesian trend filter approach of [Kowal *et al.* \(2019\)](#) to include interruptions and the detection of changepoints. Local smoothing is accomplished by specifying first or second order differences in the trend process as sparse signals through global-local shrinkage priors ([Carvalho *et al.*, 2009](#)). To diminish insignificant patterns and merge sustained trends together, while still allowing instantaneous changes, we specify a local shrinkage ‘process’ prior through a threshold stochastic volatility model, with appropriately distributed innovations. A threshold parameter establishes a self-correcting mechanism that penalizes the occurrence of consecutive changepoints within short intervals. This also allow for posterior inference of changepoint locations and size. This is all performed while also accounting for additive outliers, which we model with an ultra sparse horseshoe+ prior [Bhadra *et al.* \(2017\)](#). Finally, by combining locally estimated outlier and noise parameters we also define a posterior sample ‘local outlier score’ for labeling each observation as likely anomalous, or not.

The paper proceeds as follows. Section 2 details ABCO and our novel utilization of horseshoe priors. Section 3 contrasts ABCO with many alternative methods, including a basic horseshoe approach, PELT ([Killick *et al.*, 2012](#)), E.Divisive ([Matteson and James, 2014](#); [Zhang *et al.*, 2019](#)), Wild Binary Segmentation (WBS, [Fryzlewicz, 2014](#)), and Bayesian changepoint analysis (BCP, [Erdman and Emerson, 2008](#)), in diverse simulation scenarios. Section 4 investigates two real world applications using ABCO. Section 5 concludes with discussion of possible extensions.

2 Methodology

ABCO decomposes a time series $\{y_t\}$ as the sum three components: a local mean or trend signal $\{\beta_t\}$, a sparse additive outlier signal $\{\zeta_t\}$ and a heteroskedastic noise process $\{\epsilon_t\}$. Specifically, we have

$$y_t = \beta_t + \zeta_t + \epsilon_t, \quad \epsilon_t \sim N(0, \sigma_{\epsilon,t}^2), \quad (1)$$

where $\epsilon_t = \delta_t \sigma_{\epsilon,t}$ and $\delta_t \stackrel{iid}{\sim} N(0, 1)$. ABCO’s decomposition effectively distinguishes a potentially locally varying mean or trend signal from a complex error process $\{\zeta_t + \epsilon_t\}$ that may contain outliers and exhibit non-constant volatility. Next, we detail each of the three model components of ABCO.

We assume the noise process $\{\sigma_{\epsilon,t}^2\}$ follows a stochastic volatility (SV) model to capture potential heteroskedasticity. For simplicity, we focus on the first order SV(1) model of ([Kim *et al.*, 1998](#)) with

Gaussian innovations in log volatility. Specifically, we assume

$$\log(\sigma_{\epsilon,t}^2) = \mu_\epsilon + \phi_\epsilon[\log(\sigma_{\epsilon,t-1}^2) - \mu_\epsilon] + \xi_{\epsilon,t}, \quad \xi_{\epsilon,t} \sim N(0, \sigma_\xi^2).$$

We find this relatively simple noise model to be adequate in practice, but more complex specifications are also easily substituted into ABCO for specific applications.

By modeling measurement error using an SV(1) model, we concisely account for heteroskedastic measurement error. By supposing $\sigma_{\epsilon,t}^2$ is a constant σ_ϵ^2 for all t , we have measurement error with constant variance, which we later denote as ‘ABCO w/o SV’. As shown in Sections 3 and 4, incorporating stochastic volatility greatly improves changepoint detection in series with heteroskedastic noise, while maintaining an equal level of performance in series with constant noise variance, at minimal computational cost. This simple SV component, which has not been widely adopted in other change point models, provides ABCO with enhanced flexibility for modeling more varied and complex applications.

2.1 Local Outlier Detection and Scoring

The sparse outlier process $\{\zeta_t\}$ models large deviations at specific times, for which we suppose an independent horseshoe+ shrinkage prior, as in [Bhadra *et al.* \(2017\)](#):

$$\begin{aligned} (\zeta_t | \lambda_{\zeta,t}, \tau_\zeta, \eta_{\zeta,t}) &\sim N(0, \lambda_{\zeta,t}^2), & \tau_\zeta &\sim C^+(0, \sigma_{\tau,\zeta}), \\ (\lambda_{\zeta,t} | \tau_\zeta, \eta_{\zeta,t}) &\sim C^+(0, \tau_\zeta \eta_{\zeta,t}), & \eta_{\zeta,t} &\sim C^+(0, \sigma_{\eta,\zeta}), \end{aligned}$$

where C^+ denotes the half-Cauchy distribution, and $\sigma_{\tau,\zeta}$ and $\sigma_{\eta,\zeta}$ are hyper-parameters related to the global and local shrinkage of outliers, respectively. After conditioning on the data, the process $\{\zeta_t\}$ concentrates near zero except at locations where deviations from the mean trend are much larger in magnitude than nearby deviations. Thus, we call it a sparse outlier process. Although outliers may cluster, they are assumed *a priori* independent in this specification.

The horseshoe prior provides appropriate shrinkage, strongly shrinking ζ_t toward zero when there is no apparent outlier and largely leaving ζ_t unshrunk when there is a clear outlier. With rare outliers, the outlier process $\{\zeta_t\}$ rarely take values outside a tight neighborhood of zero. This requires a even stronger shrinkage than the horseshoe provides. The alternative horseshoe+ prior, with additional variance term $\{\eta_{\zeta,t}\}$, provides more extreme horseshoe-shaped shrinkage, allowing for large deviations from zero at only a small number of locations.

In order identify specific observations y_t as potential or likely outliers, we propose a locally adaptive outlier score o_t based on the proportion of conditional variance attributed to the outlier component ζ_t relative to the variance of the overall error $\zeta_t + \epsilon_t$. From observation Equation (1) and the additional

specification details discussed earlier, we note $\text{Var}(y_t | \beta_t, \lambda_{\zeta,t}, \sigma_{\epsilon,t}) = \lambda_{\zeta,t}^2 + \sigma_{\epsilon,t}^2$; i.e. conditional on the local trend β_t , variability is split between the outlier and heteroskedastic noise terms. We thus propose the following observational outlier score, $o_t = \tilde{E} \frac{\lambda_{\zeta,t}^2}{\lambda_{\zeta,t}^2 + \sigma_{\epsilon,t}^2}$, where \tilde{E} denotes the posterior expectation. Outlier scoring provides a single ordering of the observations with respect to their relative local deviations. We apply these scores to shade the most locally anomalous observation points in later figures. Thresholding these (temporally) marginal outlier scores is a simple approach to labeling locally outlying points, and comprehensive joint analysis of outlier scores is a promising future research direction.

2.2 Trend Filtering with Changepoints

The local mean or trend signal $\{\beta_t\}$ is specified as our primary state variable. To model a local trend we focus on modeling increments in β_t , e.g., $\Delta^D \beta_t$, where Δ^D is the D th difference operator (usually for D equal to 1 or 2), with priors that induce sparsity. We suppose the following model

$$\begin{aligned} \Delta^D \beta_t &= \omega_t, & h_t &= \log(\tau_\omega^2 \lambda_{\omega,t}^2), \\ \omega_t &\sim N(0, \tau_\omega^2 \lambda_{\omega,t}^2), & h_t &= \mu + (\phi_1 + \phi_2 s_t)(h_{t-1} - \mu) + \eta_t, \end{aligned} \quad (2)$$

where s_t is defined below and $\eta_t \stackrel{iid}{\sim} Z(\alpha, \beta, 0, 1)$, in which Z denotes the four parameter Z -distribution, and where (α, β) are hyperparameters which we fix as $(\frac{1}{2}, \frac{1}{2})$ for simplicity, see [Kowal et al. \(2019\)](#).

In Equation 3 the trend increments, i.e. the evolution error $\{\omega_t\}$, is modeled by a global-local shrinkage prior with parameters τ_ω and $\{\lambda_{\omega,t}\}$. The global parameter τ_ω establishes the overall evolution error scale while the local parameters $\{\lambda_{\omega,t}\}$ shrink evolution errors locally, with respect to the time index t . Previous work introduced a simple first-order stochastic volatility SV(1) model for the process $\{\omega_t\}$ through a first order autoregression of $\{h_t\}$ with Z -distributed innovations, and showed it produced exceptionally flexible shrinkage appropriate for adaptive trend filtering ([Kowal et al., 2019](#)).

To now allow trend filtering with abrupt breaks, i.e. isolated changepoints, we consider a similarly simple, but more flexible stochastic volatility model for $\{\omega_t\}$, a first-order *threshold* stochastic volatility TSV(1) model. This is equivalent to specifying a first order threshold autoregression for $\{h_t\}$, again with Z -distributed innovations. The proposed TSV(1) model appears in Equation 3 above, in which the zero-one threshold indicator process $\{s_t\}$ allows the volatility model to exhibit an asymmetric response, ϕ_1 versus $\phi_1 + \phi_2$, in h_t with respect to a threshold variable, which we specify as $\log(\omega_{t-D}^2)$. Specifically, for a threshold parameter γ we define

$$s_t = 1 \text{ if } \log(\omega_{t-D}^2) > \gamma, \quad \text{and } 0 \text{ otherwise.}$$

Through a SV(1) prior with Z -distributed innovations, the posterior shrinkage profile for $\{\omega_t\}$ will tend

to swing between extended periods of extreme shrinkage, in which ω_t is estimated as approximately zero, and periods of less or minimal shrinkage, in which ω_t is volatile and hence the trend β_t itself is dynamically evolving. In the presence of isolated change points in the signal β_t , which coincide with large values of $\log(\omega_t^2)$, h_t is pushed higher. When ϕ_1 is closer to one than zero, the process $\{h_t\}$ also remains higher for several periods, because of the persistence induced by strong short-term memory through the autoregression. When now applying a TSV(1) prior, with the threshold indicator s_t added, and with $\phi_2 < 0$, the process $\{h_t\}$ can immediately return to a lower level following a large value of $\log(\omega_t^2)$. Overall, use of the proposed TSV(1) specification avoids over-estimation of change points, especially in high volatility periods.

In Equation (3), if we fix $\phi_1 = \phi_2 = 0$, we have non-dynamic shrinkage, in that $\{\lambda_{\omega,t}\}$ is iid, and we refer to this special case the ‘horseshoe’ evolution model (horseshoe) in this paper, as it applies the standard horseshoe prior for the evolution error variance. In Section 3 below we compare the performance of ABCO with the horseshoe model above, and with several other popular approaches, in a comprehensive simulation study. And in Appendix 6.2 we illustrate the further use of ABCO to estimate changepoints within the parameters of a dynamic linear regression model.

2.3 Interrupted Time Series

Interrupted time series analysis refers to the study of time series in which a known event or intervention has taken effect at a specific time; the goal of the analysis is to compare the pre-intervention period series with the post-intervention period series to assess the nature and impact of the intervention. For an interrupted time series $\{\dots, y_{\pi-1}, y_{\pi}, \dots\}$ where an intervention commenced at time index π , a traditional linear interrupted time series model can be written as follows (Wagner *et al.*, 2002):

$$y_t = \alpha_0 + \alpha_1 t + \alpha_2 I_t^\pi + \alpha_3 (t - \pi + 1) I_t^\pi + e_t,$$

where α_0 and α_1 are the intercept and slope of the time trend regression pre-intervention; I_t^π is an indicator variable noting whether the time index t occurs pre-intervention ($I_t^\pi = 0$ for all $t < \pi$) or post-intervention ($I_t^\pi = 1$ for all $t \geq \pi$); α_2 is the intervention effect with respect to any level shift; and α_3 is the intervention effect associated with any change in slope after intervention. Furthermore, the noise term e_t is most commonly assumed to be iid (or autoregressive), and normally distributed with mean 0 and variance σ_e^2 . This relatively simple traditional interrupted time series model has proven broadly applicable in analyzing the effect of intervention in medication applications (Wagner *et al.*, 2002), public health policy (Bernal *et al.*, 2017), and performance based incentives (Serumaga *et al.*, 2011).

ABCO can be easily adapted to apply to an interrupted time series, but with more flexibility than a traditional approach. Explicit modeling of both outliers and heteroskedastic noise (around the in-

tervention time in particular) is achieved through maintaining the same observation decomposition $y_t = \beta_t + \zeta_t + \epsilon_t$, and specifications for $\{\zeta_t\}$ and $\{\epsilon_t\}$. ABCO's flexible trend modeling allows general nonlinear trends before and after intervention. Furthermore, ABCO allow for a more detailed characterization of the intervention effect beyond an abrupt change in level and/or slope at time π . This might include anticipatory intervention effects or an intervention effect that resulted in only a temporary change.

Now, to assess the impact of an intervention of the form above, i.e. level and/or slope changes at time π , we focus on modeling second order ($D = 2$) changes in $\{\beta_t\}$ and modify the ABCO state increment equation as follows:

$$\begin{aligned}\Delta^2\beta_t &= \omega_t + v_t, & v_\pi, v_{\pi+1} &\sim N(0, \sigma_v^2), \\ \omega_t &\sim N(0, \tau_\omega^2 \lambda_{\omega,t}^2), & v_t &= 0 \quad \text{otherwise,}\end{aligned}\tag{3}$$

where σ_v^2 is assumed to be sufficiently large to give v_π and $v_{\pi+1}$ a relatively diffuse prior. Note that we expect an intervention effect to induce a large value for $|\Delta\beta_\pi|$, and in the general case of a level and/or slope change at π a large value for $|\Delta^2\beta_\pi|$, as well as potentially for $|\Delta^2\beta_{\pi+1}|$, is expected. Thus the 'jump' terms v_π and $v_{\pi+1}$ are included to allow for such corresponding changes in the underlying trend, while the same ABCO $\{\omega_t\}$ process as introduced above in Section 2.2 is applied. The interpretation of ABCO now extends to include an abrupt disruption at time π in a trend that is otherwise estimated to be adaptively smooth locally. The magnitude of the break or change in both level and slope after the intervention is specified as a function of v_π and $v_{\pi+1}$. This and related modifications of ABCO are specifically used for series with one (or more) interruptions at one (or more, but well separated) intervention times. In Section 4.3 below we illustrate the use of this modification of ABCO to analyzing effect of smoking ban in Sicily.

2.4 Inference

We conduct posterior inference via Markov chain Markov Carlo. In particular, we define a Gibbs sampling algorithm which iteratively samples parameters from their full conditional distributions. In this section, we provide an overview of the sampling steps of ABCO. The details for the majority of these components are expanded in Appendix 6.1 as some follow closely from related work (Kowal *et al.*, 2019). The exception is the threshold variable γ , which is more difficult to estimate and sampling details are summarized below.

Let $\mathbf{Y} = [y_1, \dots, y_T]$, $\mathbf{h} = [h_1, \dots, h_T]$, $\boldsymbol{\eta} = [\eta_1, \dots, \eta_T]$, $\boldsymbol{\beta} = [\beta_1, \dots, \beta_T]$, $\boldsymbol{\sigma}_\epsilon^2 = [\sigma_{\epsilon,1}^2, \dots, \sigma_{\epsilon,T}^2]$, $\boldsymbol{\zeta} = [\zeta_1, \dots, \zeta_T]$, $\boldsymbol{\lambda}_\zeta = [\lambda_{\zeta,1}, \dots, \lambda_{\zeta,T}]$, $\boldsymbol{\eta}_\zeta = [\eta_{\zeta,1}, \dots, \eta_{\zeta,T}]$ and $\boldsymbol{\xi}_\epsilon = [\xi_{\epsilon,1}, \dots, \xi_{\epsilon,T}]$. Sampling all variables in the evolutionary equation from their full conditional involves sampling the log volatility $p(\mathbf{h}|\boldsymbol{\beta}, \phi_1, \phi_2, \mu, \gamma, \boldsymbol{\eta})$, the unconditional mean $p(\mu|\mathbf{h}, \boldsymbol{\beta}, \phi_1, \phi_2, \gamma, \boldsymbol{\eta})$, the evolution equation coefficients $p(\phi_1|\mathbf{h}, \boldsymbol{\beta}, \phi_2, \mu, \gamma, \boldsymbol{\eta})$,

$p(\phi_2|\mathbf{h}, \boldsymbol{\beta}, \phi_1, \mu, \gamma, \boldsymbol{\eta})$, the threshold $p(\gamma|\mathbf{h}, \boldsymbol{\beta}, \phi_1, \phi_2, \mu, \boldsymbol{\eta})$ and the evolution error $p(\boldsymbol{\eta}|\mathbf{h}, \boldsymbol{\beta}, \phi_1, \phi_2, \mu, \gamma)$. The state variable is sampled jointly from $p(\boldsymbol{\beta}|\mathbf{h}, \phi_1, \phi_2, \mu, \gamma, \boldsymbol{\eta}, \boldsymbol{\sigma}_\epsilon^2, \boldsymbol{\zeta}, \mathbf{Y})$. The outlier process is sampled from $p(\boldsymbol{\zeta}|\boldsymbol{\beta}, \boldsymbol{\sigma}_\epsilon^2, \boldsymbol{\lambda}_\zeta, \tau_\zeta, \boldsymbol{\eta}_\zeta, \mathbf{Y})$ along with other associated parameters using a sampler for the horseshoe prior based on the inverse gamma distribution (Makalic and Schmidt, 2016). And the observational variance is sampled from $p(\boldsymbol{\sigma}_\epsilon^2|\boldsymbol{\beta}, \boldsymbol{\zeta}, \mu_\epsilon, \phi_\epsilon, \boldsymbol{\xi}_\epsilon, \mathbf{Y})$ along with other associated variables using the stochvol R package (Hosszejni and Kastner, 2019).

The update for γ is less straightforward relative to the other parameters above. Following derivations in Nakajima and West (2013), for each time step t , marginalizing over ω_t gives $P(\log(\omega_t^2) > \gamma) = P(\omega_t > e^{\gamma/2}) = 1 - \Phi(\frac{e^{\gamma/2}}{\tau\lambda_t})$ where Φ is the CDF for standard normal distribution. From this we see that τ , $\{\lambda_t\}$ and $\{y_t\}$ play important roles in identifying an appropriate range for γ . However, the full conditional distribution for γ does not have a standard form. Despite this challenge, it is important to learn γ from the data, even in the presence of outliers, because it plays a crucial role in determining the location of the change points. After experimenting with numerous sampling schemes, including slice sampling (Neil, 2003) and a Griddy Gibbs sampler (Ritter and Tanner, 1992), we find that applying Metropolis-Hastings within a Gibbs sampler (Nakajima and West, 2013) was both simple and adequate for estimating γ within the ABCO model, allowing one to choose essentially any prior for it. We further found that a uniform prior, $\gamma \sim \text{Unif}(\ell_\gamma, u_\gamma)$, worked well provided the range was tailored to the observed data, and we relate the lower and upper limits to the volatility of the D th degree differences of the observations. Specifically, we let $\ell_\gamma = \min\{\log[(\Delta^D y_t)^2]\}$ and $u_\gamma = \max\{\log[(\Delta^D y_t)^2]\}$.

2.5 Shrinkage Profile of ABCO

As detailed above, ABCO decomposes observations y_t into three components, $(\beta_t, \zeta_t, \epsilon_t)$, i.e. trend, outlier, and noise components, respectively. Conditional on the noise and outlier components, a horseshoe like shrinkage prior is placed on the variance of the D th degree difference of the trend component. In particular, a threshold stochastic volatility model (THSV) of order 1 with Z -distributed innovations is used to model the log of the variance for the trend component increments. Without the threshold variable $\{s_t\}$ and coefficient ϕ_2 in the model, the shrinkage on $\{\beta_t\}$ follows the dynamic shrinkage process introduced in Kowal *et al.* (2019), wherein the authors detailed its shrinkage profile. Below we discuss and relate the shrinkage profile induced by the state increment variance $\{\tau_\omega^2 \lambda_{\omega,t}^2\}$ of ABCO with the dynamic shrinkage process.

Remark 1. Let $\kappa_t = (1 + \{\tau_\omega^2 \lambda_{\omega,t}^2\})^{-1}$ denote the shrinkage proportion at time t , where as $\kappa_t \rightarrow 0$ there is no shrinkage and as $\kappa_t \rightarrow 1$ there is maximal shrinkage. The following properties hold for the shrinkage of the trend component in ABCO: Let $\psi_t = (\tau_\omega^2)^{(1-\phi_1-\phi_2 s_t)} \left(\frac{1-\kappa_t}{\kappa_t}\right)^{\phi_1+\phi_2 s_t}$;

- (i) For any $\varepsilon \in (0, 1)$, $P(\kappa_{t+1} > 1 - \varepsilon | y_{t+1}, \{\kappa_s\}_{s \leq t}, s_t, \phi_1, \phi_2, \tau_\omega) \rightarrow 0$ as $\psi_t \rightarrow 0$ uniformly in $y_{t+1} \in \mathbb{R}$;

(ii) For any $\varepsilon \in (0, 1)$ and $\psi_t < 1$, $P(\kappa_{t+1} < \varepsilon | y_{t+1}, \{\kappa_s\}_{s \leq t}, s_t, \phi_1, \phi_2, \tau_\omega) \rightarrow 1$ as $|y_{t+1}| \rightarrow \infty$.

The proof for both properties can be derived analogously to the proof of Theorem 3 in [Kowal *et al.* 2019](#). The first property notes that ABCO will shrink the variance of the state equation toward 0 as $\tau_\omega \rightarrow 0$, confirming τ_ω^2 is a global shrinkage parameter in ABCO. The second property notes that a sufficiently extreme value of y_{t+1} will still lead to a large change in the underlying mean trend, and this also motivates the use of the outlier process $\{\zeta_t\}$ to redistribute the impact of such an extreme, particularly when it is isolated.

Finally, comparing the dynamic shrinkage process with ABCO, we can see that the posterior for κ_{t+1} can be written as

$$[\kappa_{t+1} | y_{t+1}, \{\kappa_s\}_{s \leq t}, s_t, \phi_1, \phi_2, \tau_\omega] = (1 - \kappa_{t+1})^{-1/2} [1 + (\psi_t - 1)\kappa_{t+1}]^{-1} \exp(-y_{t+1}^2 \kappa_{t+1} / 2).$$

Assuming all other parameters are fixed, the posterior distribution of κ_{t+1} given $s_t = 1$ has more mass near 0 in comparison to the posterior distribution of κ_{t+1} given $s_t = 0$. This further highlights the purpose of the threshold variable; $\{s_t\}$ (and ϕ_2) lowers the shrinkage value of κ_{t+1} after the occurrence of a change point. In this way, ABCO separates isolated jumps in the trend from sustained periods of evolution in the trend.

3 Simulation Experiments

3.1 Multiple Changes in Mean with Heteroskedastic Noise

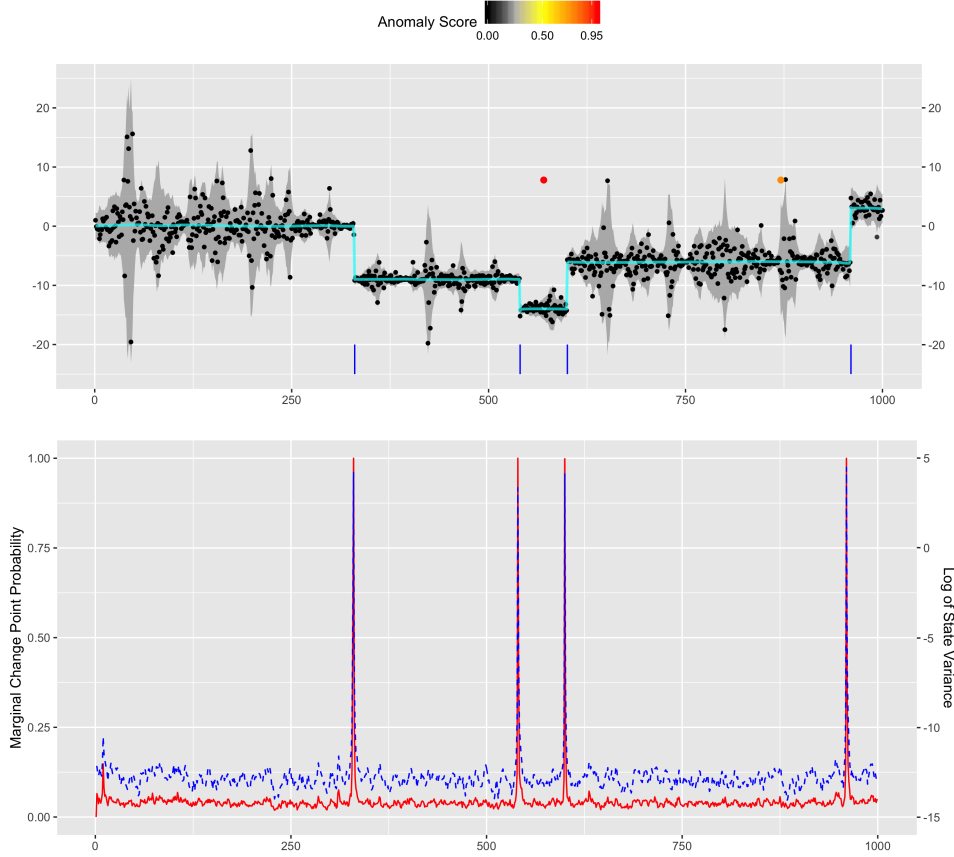
First, we consider the effectiveness of ABCO in the challenging setting of estimating multiple change-points in mean in the presence of heteroskedastic noise. In this section we generate $N = 100$ simulated series of length $T = 1000$. For each series, the number of changepoints are generated uniformly at random from the set $\{2, 3, 4\}$. Changepoint locations are uniformly sampled but with the constraint that their minimal distance is 30 time increments. The resulting segments are each assigned a mean uniformly distributed between -20 and 20 . Finally, innovations with stochastic volatility are added to the mean signals, with log volatility specified as

$$\log(\sigma_{\epsilon,t}^2) = \phi_\epsilon \log(\sigma_{\epsilon,t-1}^2) + \alpha_t, \quad \alpha_t \sim N(0, \sigma_\alpha^2), \quad (4)$$

with $\phi_\epsilon = 0.9$ and $\sigma_\alpha^2 = 1$. More simulation results for varying values of ϕ_ϵ and σ_α^2 are shown in Appendix 6.3. Figure 1 give an example of such a generated series, but with two outliers also included for illustration here (outliers are considered further below). Each series tends to have substantial local fluctuations which make change point analysis difficult. Table 1 details results comparing the performance of ABCO with

the previously defined ‘static’ Horseshoe approach, PELT (Killick *et al.*, 2012), WBS (Fryzlewicz, 2014), E.Divisive (James and Matteson, 2014), and BCP (Erdman and Emerson, 2008). E.Divisive, PELT and WBS are specified using default parameters with minimum segment length 30, and BCP is specified using default parameters, 5000 MCMC iterations, and with change points identified at times indices with posterior probability of a change point above 0.5.

Figure 1: Example Plots for Changes in Mean with Stochastic Volatility



The top plot shows an example of simulated data with two added outliers (colored in red and orange). The anomaly scoring shows local adaptive of the algorithm; the first (left) outlier (above a low volatility region) has the highest score while the second (right) outlier (above a high volatility region) has a lower score. The cyan lines indicate posterior mean of $\{\beta_t\}$; vertical blue lines indicate predicted change points and gray bands indicate 95% point-wise credible bands for the data excluding the anomaly process component. The bottom plot shows the marginal probability being a change point at each time step (red line) and $\{\log(\omega_{t-D}^2)\}$ (blue dashed line); the marginal probability at each time step t is calculated from the percentage of posterior simulations of $\log(\omega_{t-D}^2)$ that exceed the change point threshold γ . We can see, as a result of the threshold variable, $\{\log(\omega_{t-D}^2)\}$ spikes when change point is predicted and comes down right-away; this is key for not over-predicting in regions of high-volatility.

From the results shown in Table 1 we see that ABCO greatly outperforms the competing models, and highlights the lack of robustness these popular approaches have to heteroskedastic noise, as introduced in this scenario. Specifically, ABCO achieves the highest average Rand value, 0.958, and the highest adjusted Rand average of 0.912, with standard errors of 0.009 and 0.018, respectively. The static Horseshoe approach was a far second based on these metrics, with an average adjusted Rand of 0.528 (se 0.032);

Table 1: Mean Changes with Stochastic Volatility

Algorithms	Rand Avg.	Adj. Rand Avg.	Avg. Diff. CP	Avg. Dist. to True
ABCO	0.958 _(0.009)	0.912 _(0.018)	0.64 _(0.06)	0.25 _(0.04)
Horseshoe	0.688 _(0.022)	0.528 _(0.032)	1.84 _(0.15)	55.95 _(5.92)
E.Divisive	0.851 _(0.010)	0.446 _(0.034)	6.86 _(0.24)	65.07 _(4.15)
Pelt	0.684 _(0.012)	0.249 _(0.012)	73.66 _(2.25)	152.39 _(6.78)
WBS	0.633 _(0.015)	0.277 _(0.015)	83.20 _(1.28)	154.75 _(6.76)
BCP	0.716 _(0.014)	0.346 _(0.023)	59.38 _(4.30)	92.56 _(4.01)

Rand Avg. measures similarity between predicted partition and true partition; the value ranges between 0 and 1, with 1 being a perfect match. Adjusted Rand corrects Rand for random chance of predicting the correct segmentation. Avg. Diff. CP. reflects the average difference between the true and predicted number of change points. Avg. Dist. to True measures the average distance from a predicted change point to the nearest true change point. The standard error for each average is shown in subscript parentheses.

others had average adjusted Rand below 0.5.

A further statistic to highlight is the average distance from a predicted change point to a true change point. ABCO has an impressive distance of 0.25 (se 0.04), with almost every predicted change point very close to a true changepoint. While E.Divisive and PELT were similar to static Horseshoe in terms of Rand index, they have much greater prediction-to-true distance, implying many more false positives are predicted. The ability to avoid false positives in this setting makes ABCO well suited for diverse applications. In comparison, the static Horseshoe algorithm is less accurate in predicting the correct number of change points and tends to miss some more subtle change as illustrated by the average difference between the number true and predicted changepoints. This further supports the previous finding in Kowal *et al.* (2019) that the SV(1) model provides better estimation of the true mean, which in this case was piece-wise constant. PELT and WBS assume iid Gaussian errors; as a result, they tend to not perform well under this setting.

Furthermore, within the Bayesian framework, ABCO provides estimates both the local mean and point-wise credible bands. This allows tracking both a constant or varying signal within each cluster. We can see in Figure 1 that the credible bands are able to adapt well to regions of high volatility.

3.2 Detecting Changes in the Presence of Outliers

Next we illustrate the effectiveness of ABCO in the presence of significant outliers. Two scenarios of data sets are generated: series with changes in mean and series with changes in linear trend. For changes in mean, series are generated of length 100-2000, with a single change point randomly included in the middle 50 percent of the series, partitioning the series into two segments. The first segment has mean chosen uniformly at random between 0 and 5 while the second segment has mean chosen uniformly at random between 10 and 15. Both segments have noise simulated by a normal distribution with mean 0 and variance 1. Additionally, for each segment, the number of significant outliers are generated uniformly at

Table 2: Outlier Extension: Changes in Mean

Algorithms	Rand Avg.	Adj. Rand Avg.	Avg. No. CP	Avg. Dist. to True
ABCO	0.986 _(0.006)	0.971 _(0.013)	1.20 _(0.07)	12.61 _(6.40)
Horseshoe	0.738 _(0.015)	0.471 _(0.030)	3.55 _(0.25)	198.19 _(17.15)
E.Divisive	0.919 _(0.009)	0.841 _(0.018)	2.01 _(0.10)	54.60 _(7.22)
Pelt	0.743 _(0.008)	0.471 _(0.014)	5.96 _(0.18)	117.21 _(11.97)
WBS	0.682 _(0.012)	0.367 _(0.011)	14.88 _(0.06)	197.65 _(11.98)
BCP	0.637 _(0.004)	0.312 _(0.006)	15.22 _(0.08)	139.91 _(13.99)

Result for ABCO against other change point algorithms on simulated data with changes in mean and significant outliers. The metrics mostly match those detailed in Table 1, except Avg. No. CP. which measures the average number of change points predicted by the algorithm (truth is 1).

Table 3: Outlier Extension: Linear Trend Results for ABCO

Outlier Type	Rand Avg.	Adj. Rand Avg.	True Positive Rate	False Positive Rate
Small	0.954 _(0.014)	0.908 _(0.029)	0.705 _(0.040)	0.001 _(0.0001)
Large	0.949 _(0.015)	0.897 _(0.030)	0.951 _(0.015)	0.001 _(0.0005)
Mixed	0.939 _(0.016)	0.878 _(0.033)	0.921 _(0.021)	0.001 _(0.0002)

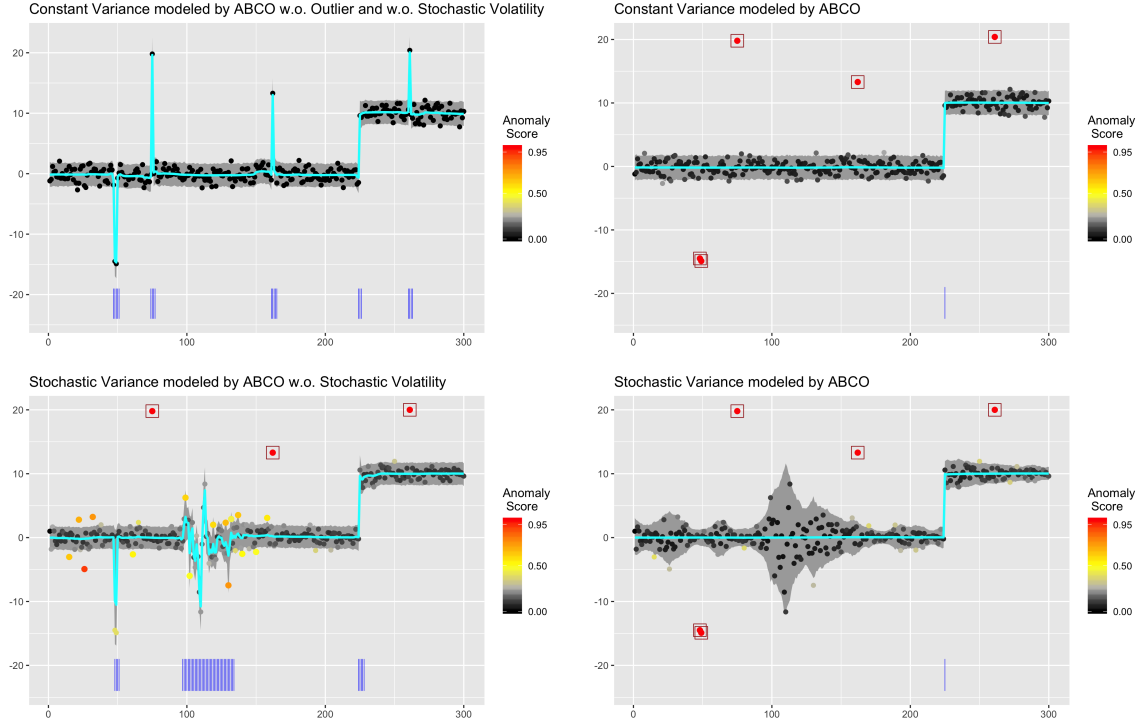
Result for ABCO on predicting both change points and outliers in linear settings. Average Rand and adjusted Rand reflect accuracy of change point detection, while true positive and false positive rates measures accuracy of outlier detection. The standard error for all measurement are shown in parentheses.

random from the set $\{5, 6, 7, 8, 9, 10\}$ and each outlier is chosen uniformly at random to be 5-30 standard deviations away from the mean. We again fit the ABCO model, the static horseshoe model, E.Divisive, PELT, WBS and BCP on the simulated data sets; results are shown in Table 2.

For ABCO, outliers are flagged using the outlier scoring detailed in Section 2.1. We choose a cutoff threshold 0.95 for $\{o_t\}$. Figure 2 shows the effectiveness of local outlier scoring in the presence of stochastic volatility within ABCO. As shown, modeling stochastic volatility within ABCO increases its effectiveness while maintaining the same level of performance for series with constant variance. Hence, we recommend including both outlier and heteroskedastic noise when deploying ABCO, in general.

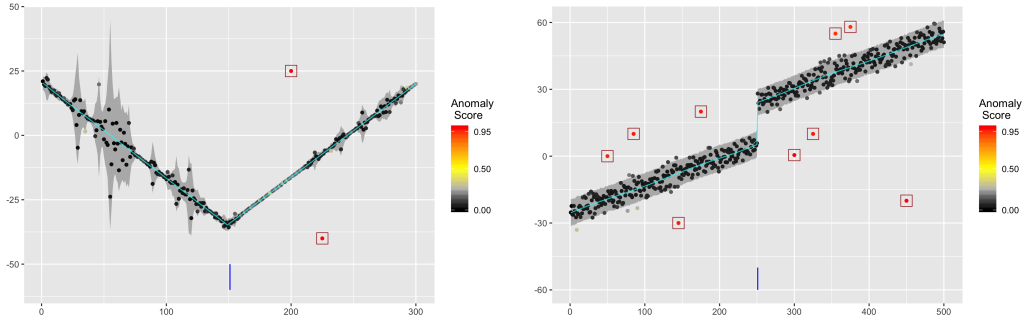
For changes in linear trend, series are generated with a length of 100 with a change point randomly selected in the middle 20% of the data. The linear ‘meet-up’ model is utilized to generate the data, meaning the segments are set to be continuous (end of segment 1 becomes the start of segment 2). The start and end of segment 1 as well as end of segment two are uniformly randomly generated between -100 and 100. The segments are set to have a minimum slope difference of 1.5 to ensure identifiability. Three types of outlier settings are generated: small (5-10 std. dev. away from the true mean), large (25-30 std. dev. away from the true mean) and mixed (5-30 std. dev. away from the true mean). We generate $N = 100$ series for each outlier setting, with 5-10 outliers randomly generated for each segment. Since only the ABCO algorithm can effectively deal with linear trends in presence of outliers, we ran the ABCO algorithm in each of the three settings and reported the results terms of both change point detection accuracy and outlier detection accuracy.

Figure 2: Anomaly Scores with Outliers



This figure illustrates data generated with same signal and outlier but different noise processes. The top plots are generated with constant noise variance while the bottom plots are generated with stochastic noise variance. The top left plot show results generated by running the ABCO model without (w.o.) the outlier component and without stochastic volatility. The bottom left plot shows results generated by running ABCO model without stochastic volatility. As seen in plots above, ABCO struggles to adapt to these series without these two model components included. True positive outliers flagged by the model are outlined by squares. The estimated mean (trend) is shown in cyan; estimated change point locations are indicated by blue vertical lines below the series, and credible bands for the observations excluding the estimated outlier process is shown in gray.

Figure 3: Linear Data Examples



Examples of plots generated using simulated series with linear trends, change points and outliers. Left figure shows an example of a linear meet-up model generated with stochastic volatility and 2 outliers. Right figure shows a common linear trend with a jump and several outliers. Outlier scoring is calculated by the ABCO model with true positive outliers outlined by squares. Vertical lines below the series indicate estimated change point locations; cyan line denote the estimated mean (trend) with 95% credible bands for the estimated signal plus noise (excluding the estimated outlier component) in gray.

The first simulation scenario is summarized in Table 2, where it is clear that ABCO again substantially outperforms other models. ABCO consistently achieves an average Rand value of at least 0.986 (se 0.006) and an adjusted Rand value around 0.971 (se 0.013). E.Divisive came second with adjusted rand of 0.841

(se 0.030), while all other algorithms performed quite a bit worse. This demonstrates the robustness of the ABCO algorithm in dealing with isolated outliers. For penalized likelihood algorithms such as PELT, if the outliers become large enough, they will be treated as change points. A Bayesian algorithm such as BCP, without a clear means to account for outliers, also does not work well for on this type of data. Clustered outliers are especially difficult for these algorithms to deal with as they mimic the occurrence of a new cluster and they also break the Gaussian noise assumption. By utilizing a horseshoe plus prior for $\{\zeta_t\}$, ABCO is able to adapt to large outliers that significantly deviate from the data and not treat bursts of outliers as change points.

In the linear trend simulation scenario, we illustrate the effectiveness of ABCO in flagging locations of outliers in the data. By using the local outlier scoring metric proposed in Section 2.1, ABCO is able to have a high true positive rate and a low false positive rate for all three types of outliers (an example of outlier scoring is seen in Figure 3). As shown in Table 3, ABCO is able to maintain an average adjusted Rand value of at least 0.878, signaling its effectiveness in identifying true change points. The detection of both change points and outliers simultaneously allows ABCO to provide more information for analysis. As we can see in figure 3, a series may contain a significant amount of outliers, a very difficult or impossible setting for other changepoint algorithm. The ability to incorporate both heteroskedastic noise and outlier detection makes ABCO very widely applicable. More simulation scenarios for ABCO including varying signal-to-noise ratios and dynamic regression analysis are shown in Appendix 6.3.

4 Illustrative Applications

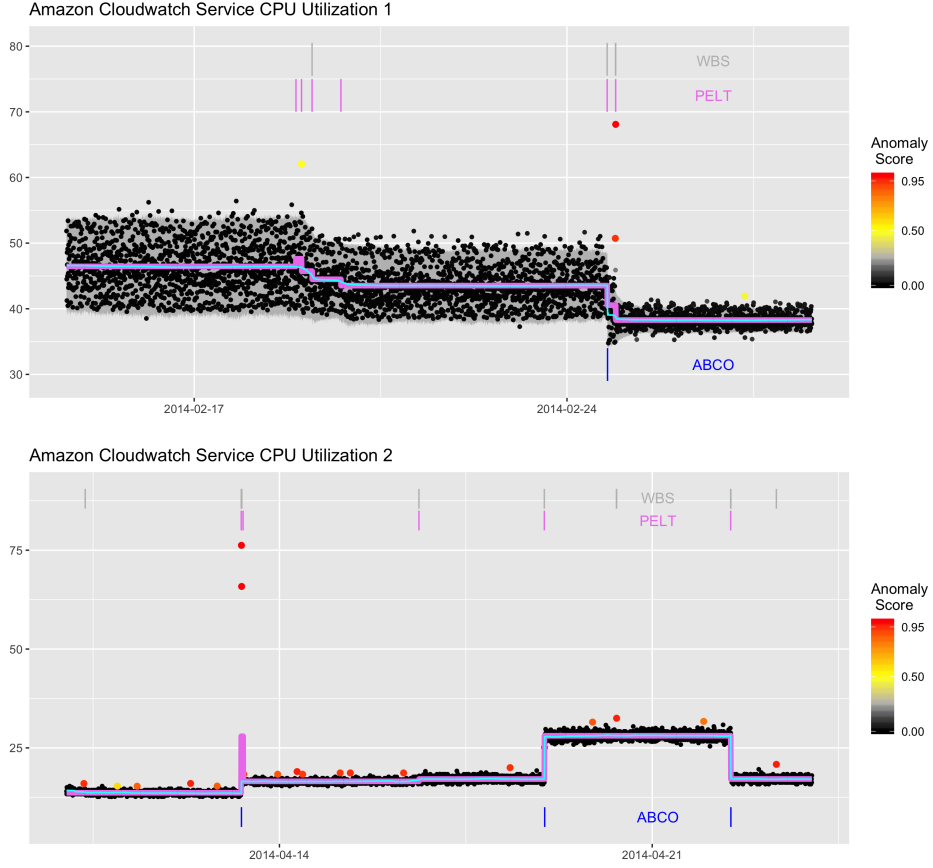
4.1 Amazon Cloudwatch Server Metrics

For our first illustrative application we consider time series from the Numenta Anomaly Benchmark (Ahmad *et al.*, 2017). Each series considers CPU utilization server metrics on Amazon Cloudwatch, and contains both changepoints and anomalies. Figure 4 illustrates two such series, and two more are shown in Appendix 6.4. Each series exhibits changes in trend, local and global anomalies, and non-constant volatility, and nicely highlights the utility and robustness of ABCO. We also compare ABCO estimates with both WBS and PELT in terms of change points and trend estimation.

As shown in Figure 4, ABCO performs well in this complicated setting. Both PELT and WBS tend to over-predict the number of change points in the series and chase significant point anomalies. As seen in the top plot, ABCO differentiates gradual shifts in mean from abrupt change points. PELT and WBS over-predict change points in regions where there are slight changes in trend. ABCO’s local adaptability effectively handles such features without over-predict the number of change point.

Additionally, ABCO is very robust to the presence of potential outliers, whereas extreme outliers force both PELT and WBS to explain them as changepoints. ABCO estimates an outlier signal to model

Figure 4: AWS CPU Utilization Results



Figures show two AWS CPU utilization series with estimates from ABCO, WBS and PELT. The cyan line represents predicted signal from the ABCO algorithm and purple line represents predicted mean from PELT. Change points from the ABCO are shown by blue vertical bars below the series; change points from PELT and WBS are shown by purple and gray vertical bars, respectively, above the series. Dark gray bands represent credible bands produced by ABCO's estimate of signal plus noise (estimated outlier process excluded), which are especially relevant for ABCO local outlier scoring, which is indicated by observation shading.

them effectively without affecting the underlying trend model. As seen in Figure 4, in the presence of significant outliers, both WBS and PELT predict an additional change point in the second half of the top series and in the first half of the bottom series. This example highlights ABCO's ability to adapt to real world data and predict true change points without over-predicting in presence of outliers or smooth local trends.

4.2 Political Approval Ratings

For another illustrative application we consider the polling data for George W. Bush's approval rating from 2000 to 2008. The series is made available on Gallup's website and has been previously analyzed by [Ratkovic and Eng \(2010\)](#). Identifying key trends in the polling data has become an important area for political analysis ([Keele, 2008](#)). Understanding when the underlying trends of a polling approval rate shifts can be very important in political decision making. The top panel in Figure 5 shows the recorded

approval ratings. As shown, there are clear long term linear trends with two significant jumps attributed to 9/11 and the invasion of Iraq. However, the jumps along with changing variability in the polling data make performing changepoint analysis difficult. Any model without the ability to account for breaks in trend will struggle to deal with this series. Additionally, the polls are taken at irregular time intervals. To transform the data into equally spaced time points, we utilize a two week moving average, similar to preprocessing done in [Ratkovic and Eng \(2010\)](#), who also handled missing points by imputing using an average of the neighboring points. With this minimal amount of pre-processing the original structure remains. It is possible to extend ABCO for unequally spaced observations in future work.

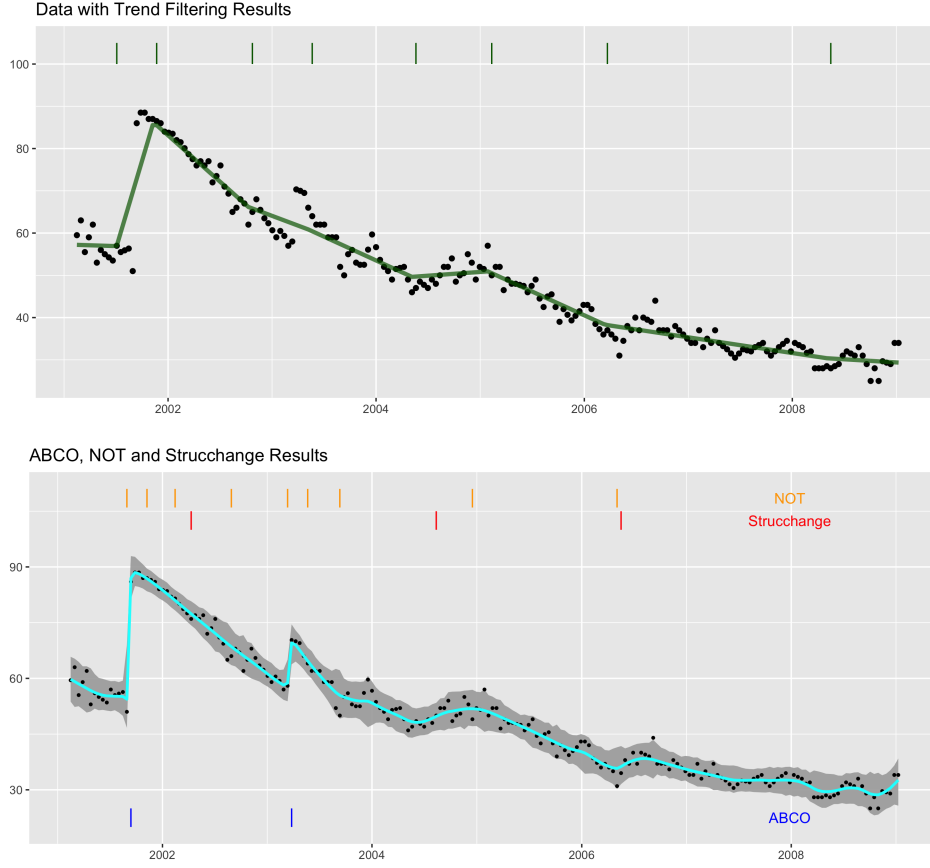
We first contrast the resulting predicted trend of ABCO with those from a trend filtering estimate using the R package `genlasso` ([Tibshirani and Taylor, 2011](#)). As seen in the top panel of figure 5, this trend filtering estimate struggles to deal with the sharp jumps and local variability of the underlying trend. As a result, the estimate overfits the data and over-estimates the number of changepoints. ABCO gives the best estimate of the underlying trend by predicting the jumps as changepoints and fitting a relatively smooth path everywhere else. As the underlying data is not perfectly linear due to the fluctuating nature of polling, the ability of ABCO to account for these small local fluctuations over time allow it to outperform other algorithms.

Next, we compared the changepoints predicted by ABCO with those from algorithms `strucchange` ([Zeileis et al., 2002](#)) and narrowest-over-threshold (NOT, [Baranowski et al., 2019](#)). `Strucchange` estimates structural changes in linear regression through a generalized fluctuation test. NOT is a non-parametric method that utilizes a series of generalized likelihood ratio test to produce the best segmentation for the data. In addition, we ran `E.divisive` and `BCP` on the first degree difference of the observations. ABCO predicts two changepoints, one after the event of 9/11 and one after the event of Iraq War. The `strucchange` algorithm finds 3 changepoints however they do not align with the jumps. This is because the `strucchange` algorithm attempts to fit continuous piecewise linear segments on the data and cannot deal with jumps in the underlying trend. NOT overfits the data and predicts 9 changepoints due to its inability to account for local fluctuation. `E.Divisive` predicts no changepoints and `BCP` significantly over-predicts the number of changepoints, but we acknowledge that finding changepoint from only first degree difference is a more difficult task. Overall, ABCO is the only algorithm that correctly identifies changepoints after the significant events and not over-predict anywhere else.

4.3 Rate of Acute Coronary Events in Italy

For an illustration of applying ABCO to an interrupted time series, we additionally consider the effect of a smoking ban in Sicily, Italy on the hospital admission rate for acute coronary events (ACE) ([Barone-Adesi et al., 2011](#)). Monthly ACE rate is recorded from 2002 to 2006 with a smoking ban taking place January of 2005. The dataset has been previously analyzed using interrupted time series in [Bernal et al.](#)

Figure 5: Approval Rating of George W. Bush

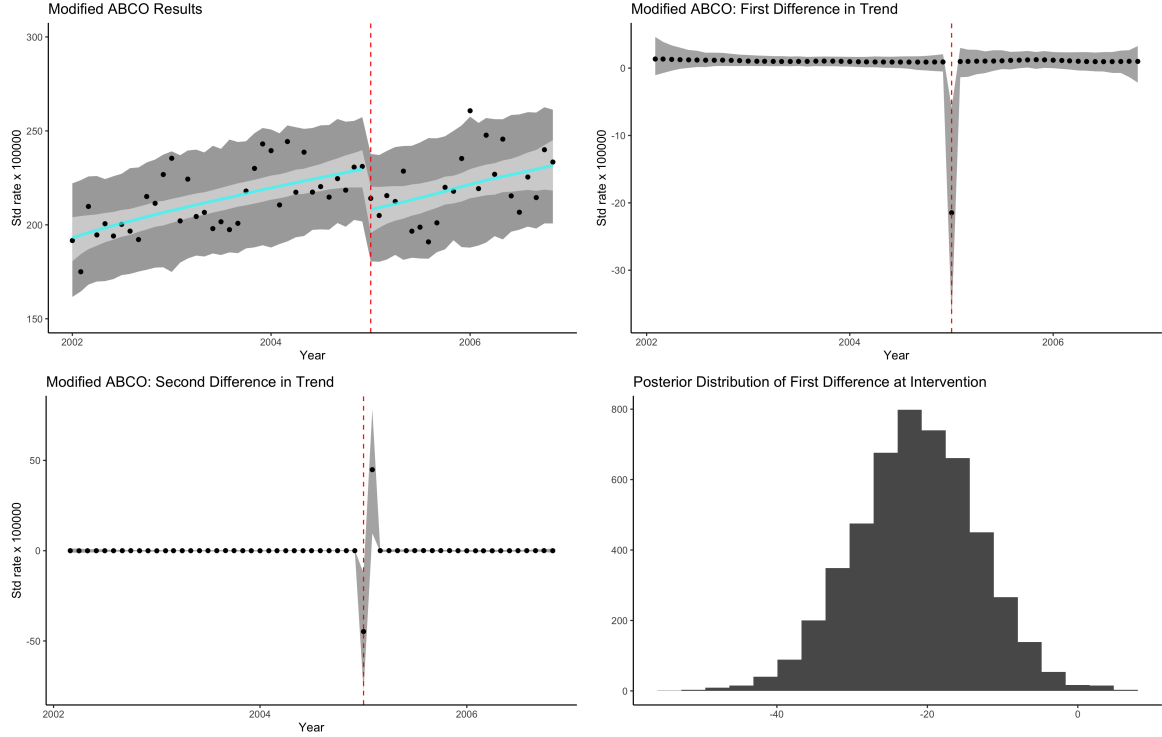


The top panel shows the polls of approval ratings for George W. Bush from 2000 to 2008 along with estimated trend from first order trend filtering (shown in green). The bottom panel shows result of running ABCO, Strucchange and NOT on the approval rating series. Change points found by ABCO, Strucchange and NOT are shown in blue, red and orange vertical bars, respectively. Dark gray credible bands for the estimated signal plus noise are produced by ABCO with the cyan line representing the local mean trend predicted by ABCO.

(2017). The series is shown in Figure 6, with the results of applying the modified ABCO method. The most prominent feature is a major level shift in the underlying trend after the smoking ban in January of 2005, but the slope (rate of increase over time) before and after the intervention appears very similar.

Our overall conclusions in this case are very similar to the finding of traditional interrupted time series analysis (Bernal *et al.*, 2017). Some of the advantages the modified ABCO provides is flexibility in estimating the trends pre- and post-intervention; robustness to any outliers or heteroskedastic noise; adaptive uncertainty quantification over time and at the intervention time in particular. We note from the figure that there is roughly constant variability in changes in the trend (although slightly larger post intervention) except at time π where ABCO has estimated substantially more uncertainty about the intervention effect size. This is highlighted in the right panel which shows the estimated posterior distribution for $\Delta\beta_\pi$ which is centered around -20, but with substantial variability. Additional standard model checking was performed but not shown.

Figure 6: Effect of Smoking Ban on Rate of Acute Coronary Events in Sicily, Italy



The top-left panel shows the standardized rate of ACE over time, with the estimated modified ABCO model for interrupted time series. The posterior mean trend for $\{\beta_t\}$ is shown in cyan along with 95% credible bands for $\{\beta_t\}$ in light gray and 95% credible bands for $\{y_t\}$ in dark gray. The estimated trend appears to be linear before and after the intervention data, with a level shift downward, but with little change in slope. The top-right panel shows the first degree difference in the trend $\{\Delta\beta_t\}$ from the modified ABCO ($\{\Delta^2\beta_t = \omega_t + v_t\}$) along with 95% credible bands in dark gray. With the single departure from the otherwise constant increments we have no evidence of anticipatory or temporary intervention effects; the intervention appears to have only had an immediate, but sustained impact, in intercept in this case. The bottom-left panel shows the second degree difference in the trend $\{\Delta\beta_t\}$ from the modified ABCO along with 95% credible bands in dark gray. The negative departure at time π and the positive bounce-back of similar magnitude at time $\pi + 1$ further support the claim of a shift in intercept but not in slope at time of intervention. The bottom-right panel shows the posterior distribution of the first difference of $\{\beta_t\}$ at the intervention time π (i.e. $\Delta\beta_\pi$). From here the modified ABCO approach allows model-based inference on the effect size at intervention.

5 Conclusion

We have proposed an adaptive Bayesian changepoint model with the ability to detect multiple change points within a time series. The model separates the series at each time-step into a trend component, an outlier component and a noise component. For trend estimation with breaks, a horseshoe-like shrinkage is placed on the D th difference of the trend component through a threshold stochastic volatility model with Z -distributed innovations. This shrinkage ensures most increments are relatively small or even nearly zero while allowing some isolated changes to be significantly large. The threshold variable is used to classify large changes as change points. For the outlier component, a horseshoe-plus prior is utilized to model extreme values in the data. For the noise component, a stochastic volatility model is specified to adapt both change and outlier detection to regions of both high and low volatility, whether stochastic or not. Together, all three components allow great flexible adaptive trend modeling, change detection,

and outlier scoring.

Through simulation experiments and illustrative applications we have highlighted the unique strengths of ABCO and shown settings where it outperform competing methods, i.e. changepoint series with significant outliers and/or non-constant variance. With a Bayesian framework, ABCO provides a reliable means for simultaneously estimating changepoints and scoring anomalies, and it can be further extended, as we demonstrated in interrupted time series analysis and dynamic regression specifications. Further directions include analysis of multivariate series and incorporating covariates into change and outlier detection equations.

References

- Adams, R. P., and MacKay, D. J. (2007). “Bayesian online changepoint detection,” .
- Ahmad, S., Lavin, A., Purdy, S., and Agha, Z. (2017). “Unsupervised real-time anomaly detection for streaming data,” *Neurocomputing* **262**, 134–147.
- Aminikhanghahi, S., and Cook, D. J. (2017). “A survey of methods for time series change point detection,” *Knowl Inf Syst.* **51**, 339–367.
- Baranowski, R., Chen, Y., and Fryzlewicz, P. (2019). “Narrowest-over-threshold detection of multiple change points and change-point-like features,” *Journal of the Royal Statistical Society, Series B* **81**, 649–672.
- Barone-Adesi, F., Gasparrini, A., Vizzini, L., Merletti, F., and Richiardi, L. (2011). “Effects of italian smoking regulation on rates of hospital admission for acute coronary events: a country-wide study,” *PLoS One* **6**.
- Bernal, J. L., Cummins, S., and Gasparrini, A. (2017). “Interrupted time series regression for the evaluation of public health interventions: a tutorial,” *International Journal of Epidemiology* **46**, 348–355.
- Bhadra, A., Datta, J., Polson, N. G., and Willard, B. (2017). “The horseshoe+ estimator for ultra sparse signals,” *Bayesian Analysis* **12**, 1105–1131.
- Braun, J., Braun, R., and Müller, H.-G. (2000). “Multiple changepoint fitting via quasilikelihood, with application to dna sequence segmentation,” *Biometrika* **87**, 301–314.
- Carvalho, C. M., Polson, N. G., and Scott, J. G. (2009). “Handling sparsity via the horseshoe,” *AISTATS* **5**, 73–80.

- Chen, G., Lu, G., Shang, W., and Xie, Z. (2019). “Automated change-point detection of eeg signals based on structural time-series analysis,” *IEEE Access* **7**.
- Chen, J., and Gupta, A. (1997). “Testing and locating variance changepoints with application to stock prices,” *Journal of American Statistics Association* **92**, 739–747.
- Cho, H., and Fryzlewicz, P. (2015). “Multiple-change-point detection for high dimensional time series via sparsified binary segmentation,” *J. R. Statist. Soc. B* **77**, 475–507.
- Ebrahimzadeh, Z., Zheng, M., Karakas, S., and Kleinberg, S. (2019). “Pyramid recurrent neural networks for multi-scale change-point detection,” .
- Erdman, C., and Emerson, J. W. (2008). “A fast bayesian change point analysis for the segmentation of microarray data,” *Bioinformatics* **24**, 2143–2148.
- Fearnhead, P., and Rigaiil, G. (2017). “Changepoint detection in the presence of outliers,” *Journal of American Statistical Association* **114**, 169–183.
- Fryzlewicz, P. (2014). “Wild binary segmentation for multiple change-point detection,” *Annals of Statistics* **42**, 2243–2281.
- Giordani, P., Kohn, R., and Dijk, D. v. (2007). “A unified approach to nonlinearity, structural change, and outliers,” *Journal of Econometrics* **137**, 112–133.
- Hosszejni, D., and Kastner, G. (2019). “Modeling univariate and multivariate stochastic volatility in r with stochvol and factorstochvol,” .
- James, N. A., and Matteson, D. S. (2014). “ecp: An r package for nonparametric multiple change point analysis of multivariate data,” *Journal of Statistical Software* **62**.
- Kastner, G., and Fruhwirth-Schnatter, S. (2014). “Ancillarity-sufficiency interweaving strategy (asis) for boosting mcmc estimation of stochastic volatility models,” *Computational Statistics and Data Analysis* **76**, 408–423.
- Kawahara, Y., Yairi, T., and Machida, K. (2007). “Change-point detection in time-series data based on subspace identification,” *7th IEEE International Conference on Data Mining* 559–564.
- Keele, L. (2008). “Semiparametric regression for the social sciences,” London: Wiley and Sons .
- Killick, R., Fearnhead, P., and Eckley, I. (2012). “Optimal detection of changepoints with a linear computational cost,” *Journal of American Statistical Association* **107**, 1590–1598.
- Kim, S., Shephard, N., and Chib, S. (1998). “Stochastic volatility: Likelihood inference and comparison with arch models,” *Review of Economic Studies* **65**, 361–393.

- Kowal, D., Matteson, D., and Ruppert, D. (2019). “Dynamic shrinkage process,” *J. R. Statist. Soc. B* **81**.
- Liu, S., Yamada, M., Collier, N., and Sugiyama, M. (2013). “Change-point detection in time-series data by relative density-ratio estimation,” *Neural Networks* **43**, 72–83.
- Makalic, E., and Schmidt, D. F. (2016). “A simple sampler for the horseshoe estimator,” *IEEE Signal Processing Letters* **23**.
- Matteson, D. S., and James, N. A. (2014). “A nonparametric approach for multiple change point analysis of multivariate data,” *Journal of the American Statistical Association* **109**, 334–345.
- Mccausland, W., Miller, S., and Pelletier, D. (2011). “Simulation smoothing for state-space models: A computational efficiency analysis,” *Computational Statistics and Data Analysis* **55**, 199–212.
- Montanez, G. D., Amizadeh, S., and Laptev, N. (2015). “Inertial hidden markov models: Modeling change in multivariate time series,” *AAAI* 1819–1825.
- Nakajima, J., and West, M. (2013). “Bayesian analysis of latent threshold dynamic models,” *Journal of Business and Economic Statistics* **31**, 151–164.
- Neil, R. (2003). “Slice sampling,” *The Annals of Statistics* **31**, 705–767.
- Omori, Y., Chib, S., Shephard, N., and Nakajima, J. (2007). “Stochastic volatility with leverage: Fast and efficient likelihood inference,” *Journal of Econometrics* **140**, 425–449.
- Polson, N. G., Scott, J. G., and Windle, J. (2013). “Bayesian inference for logistic models using polya-gamma latent variables,” *Journal of the American Statistical Association* **108**, 1339–1349.
- Ratkovic, M. T., and Eng, K. H. (2010). “Finding jumps in otherwise smooth curves: Identifying critical events in political processes,” *Polit Anal.* **18**, 57–77.
- Rehman, M. H. u., Liew, C. S., Abbas, A., Jayaraman, P. P., Wah, T. Y., and Khan, S. U. (2016). “Big data reduction methods: A survey,” *Data Sci. Eng.* **1**, 265–284.
- Ritter, C., and Tanner, M. A. (1992). “Facilitating the gibbs sampler: The gibbs stopper and the griddy-gibbs sampler,” *Journal of the American Statistical Association* **87**, 861–868.
- Saatçi, Y., Turner, R., and Rasmussen, C. E. (2010). “Gaussian process change point models,” *ICML 10 Proceedings of the 27th International Conference on International Conference on Machine Learning* 927–934.
- Serumaga, B., Ross-Degnan, D., Avery, T., Elliott, R., Majumdar, S. R., Zhang, F., and Soumerai, S. (2011). “Effect of pay for performance on the management and outcomes on hypertension in the united kingdom: Interrupted time series study,” *BMJ* **342**.

- Solow, A. (1987). “Testing for climate change: An application of the two-phase regression model,” *Journal of Climate and Applied Meteorology* **26**.
- Tan, B. A., Gerstoft, P., Yardim, C., and Hodgkiss, W. S. (2015). “Change-point detection for recursive bayesian geoacoustic inversions,” *The Journal of the Acoustical Society of America* **137**, 1962–1970.
- Tibshirani, R. J., and Taylor, J. (2011). “The solution path of the generalized lasso,” *Annals of Statistics* **39**, 1335–1371.
- Wagner, A. K., Soumerai, S. B., F., Z., and Ross-Degnan, D. (2002). “Segmented regression analysis of interrupted time series studies in medication use research,” *Journal of Clinical Pharmacy and Therapeutics* **27**, 299–309.
- Zeileis, A., Leisch, F., Hornik, K., and Kleiber, C. (2002). “Strucchange: An r package for testing for structural change in linear regression models,” .
- Zhang, W., Gilbert, D., and Matteson, D. S. (2019). “Abacus: Unsupervised multivariate change detection via bayesian source separation,” *Proceedings of the 2019 SIAM International Conference on Data Mining* .

6 Appendix

6.1 MCMC Sampling Algorithm Details

In this subsection, we will expand upon the Section 2.4 summary of the MCMC sampling algorithm and detail the implementation for the remaining ABCO model parameters.

6.1.1 Sampling the log evolution variance $\{h_t\}$

To sample the log evolution variance, we will use a similar sampling method as detailed in [Kastner and Fruhwirth-Schnatter \(2014\)](#). In details below, we will describe the setup for $D = 1$; the sampler for $D = 2$ follows similarly.

As seen in Equation 3, the evolutionary log variance equation is then given by $h_{t+1} = \mu + (\phi_1 + \phi_2 s_t)(h_t - \mu) + \eta_{t+1}$. To sample the log-volatility $\{h_t\}$, we will first define $z_t = \log(\omega_t^2 + c)$. Since each ω_t follows a Gaussian distribution conditionally, each ω_t^2 follows a chi-squared distribution, conditionally. To sample the log of a chi-squared distribution, we use the 10-component discrete mixture approximation with mean, variance and weights denoted by m_i, v_i, w_i for $i \in \{1, \dots, 10\}$ ([Omori et al., 2007](#)). The discrete mixture indicators r_t are sampled in the same manner as in [Kim et al. \(1998\)](#). The joint likelihood for all h_1, \dots, h_T as follows: $\mathbf{z} \sim N(\mathbf{m} + \tilde{\mathbf{h}} + \mathbf{u}, \mathbf{\Sigma}_v)$ where $\mathbf{z} = (z_1, \dots, z_T)$, $\mathbf{m} = (m_{r_1}, \dots, m_{r_T})$, $\tilde{\mathbf{h}} = (h_1 - \mu, \dots, h_T - \mu)$, $\mathbf{\mu} = (\mu, (1 - \phi_1 - \phi_2 s_2)\mu, \dots, (1 - \phi_1 - \phi_2 s_T)\mu)$, and $\mathbf{\Sigma}_v = \text{diag}(v_{r_1}, \dots, v_{r_T})$. The

evolution equation can be written as $D\tilde{\mathbf{h}} \sim N(\mathbf{0}, \mathbf{\Sigma}_\xi)$ where $\mathbf{\Sigma}_\xi = \text{diag}(\xi_1, \dots, \xi_T)$ and $\{\xi_t\}$ is detailed in appendix 6.1.2. D is a $T \times T$ matrix with 1 on the diagonal, $(-(\phi_1 + \phi_2 s_2), \dots, -(\phi_1 + \phi_2 s_T))$ on the first off-diagonal and 0 elsewhere.

With the above setup, we can calculate the parameters of the full conditional distribution for $\tilde{\mathbf{h}}$ using the *all without a loop sampler* detailed in [McCauley et al. \(2011\)](#). The full conditional distribution is given by: $\tilde{\mathbf{h}} \sim N(\mathbf{Q}^{-1}\mathbf{l}, \mathbf{Q}^{-1})$ where \mathbf{Q} is a symmetric tridiagonal matrix with main diagonal entries \mathbf{Q}_0 and off-diagonal entries \mathbf{Q}_1 given by

$$\begin{aligned}\mathbf{Q}_0 &= [(v_{r_1}^{-1} + \xi_1 + (\phi_1 + \phi_2 s_2)^2 \xi_2), \dots, (v_{r_{T-1}}^{-1} + \xi_{T-1} + (\phi_1 + \phi_2 s_T)^2 \xi_T), (v_{r_T}^{-1} + \xi_T)] \\ \mathbf{Q}_1 &= [-(\phi_1 + \phi_2 s_2) \xi_2), -((\phi_1 + \phi_2 s_3) \xi_3) \dots, -((\phi_1 + \phi_2 s_T) \xi_T)] \\ \mathbf{l} &= [\frac{z - m_{r_1} - \mu}{v_{r_1}}, \frac{z - m_{r_2} - \mu}{v_{r_2}}, \dots, \frac{z - m_{r_T} - \mu}{v_{r_T}}]\end{aligned}$$

With the full conditional distribution derived above, we sample $\tilde{\mathbf{h}}$ using the *backhand-substitution method* detailed in [Kastner and Fruhwirth-Schnatter \(2014\)](#).

6.1.2 Sampling the remaining parameters

Since a horseshoe prior is used for the evolution error, we propose the following prior for τ_ω : $\tau_\omega \sim C^+(0, \frac{1}{\sqrt{T}})$. Using Pólya-Gamma mixing parameter as seen in [Polson et al. \(2013\)](#), the prior for μ is given by: $[\mu|\tau] \sim N(\log(\frac{1}{T}), \xi_\mu^{-1})$, where $\xi_\mu \sim PG(0, 1)$. Given that $h_1 \sim N(\mu, \xi_0^{-1})$ where $\xi_0 \sim PG(0, 1)$, the full conditional distribution for μ can be derived from formula for conjugate normal prior. The full conditional distribution is given by: $\mu \sim N(Q_\mu^{-1}l_\mu, Q_\mu^{-1})$, where

$$\begin{aligned}Q_\mu &= \xi_\mu + \xi_0 + \sum_{t=1}^{T-1} (1 - \phi_1 - \phi_2 s_{t+1}) \xi_t, \\ l_\mu &= \xi_\mu \log(\frac{1}{T}) + \xi_0 h_1 + \sum_{t=1}^{T-1} (1 - \phi_1 - \phi_2 s_{t+1}) (h_{t+1} - (\phi_1 + \phi_2 s_{t+1}) h_t).\end{aligned}$$

For ϕ_1 , assume a prior $\frac{\phi_1+1}{2} \sim \text{Beta}(20, 1)$, which restricts $|\phi_1| \leq 1$. The full conditional distribution is then sampled using a slice sampler with a lower limit of 0 and an upper limit of 1 ([Neil, 2003](#)). Slice sampling provides an effective way to sample a univariate distribution with known lower and upper limit. The full conditional is given by:

$$f_{(\phi_1+1)/2}(x) = [-\frac{1}{2} \sum_{t=1}^{T-1} (\tilde{h}_{t+1} - (2x - 1 + \phi_2 s_{t+1}) \tilde{h}_t)^2] + \text{dBeta}(x, 20, 1)$$

where $\text{dBeta}(x, 10, 2)$ is the pdf of the beta distribution with parameters $\alpha = 10$ and $\beta = 2$.

For ϕ_2 , we assume a prior truncated normal distribution with lower bound of 0, $\phi_2 \sim N(-1, 0.5) \mathbf{1}_{\phi_2 \leq 0}$. We restrict ϕ_2 to be negative as ϕ_2 functions as a negative buffer after discovering a change point. The

full conditional can be calculated by defining $\mathbf{s} = \{t; s_{t+1} = 1\}$; it is given by:

$$f_{\phi_2}(x) = \left[-\frac{1}{2} \sum_{t \in \mathbf{s}} (\tilde{h}_{t+1} - (\phi_1 + x s_{t+1}) \tilde{h}_t)^2\right] + \text{dNorm}(x, -1, 0.5)$$

where $\text{dNorm}(x, -1, 0.5)$ is the pdf of the normal distribution with mean -1 and standard deviation of 0.5 . The full conditional distribution is sampled with lower limit of -5 and upper limit of 0 .

The evolution error $\{\eta_t\}$ is defined by a Pólya-Gamma hierarchical parameterization (Polson *et al.* (2013)) given by $[\eta_t | \xi_t] \stackrel{\text{ind.}}{\sim} N(0, \xi_t^{-1})$ where $\xi_t^{-1} \sim PG(1, 0)$. The Pólya-Gamma parameters, $\{\xi_t\}$, are sampled using the `rpg()` function from Bayeslogic R package. Next, the state variable $\{\beta_t\}$ is sampled in a similar manner as in Kowal *et al.* (2019). Lastly, the observation variance ϵ_t follow a standard stochastic volatility model. The observational variances are sampled using `stochvol` R package.

6.2 ABCO-X / Extension for Dynamic Regression

Through the Bayesian inference framework, the ABCO model can easily be extended to the case of non-intercept, and multiple explanatory predictors. In particular, this extension allows for identification of change points within a varying coefficient regression problem. We call this extension ABCO-X.

Let $\mathbf{x}_t = (x_{1,t}, \dots, x_{p,t})$ be p predictors for y_t , then the ABCO-X model can be expressed as follows:

$$y_t = \mathbf{x}_t' \boldsymbol{\beta}_t + \zeta_t + \epsilon_t \quad (5)$$

$$\Delta^D \boldsymbol{\beta}_t = \boldsymbol{\omega}_t \quad \omega_{j,t} \sim N(0, \tau_{\omega,0}^2 \tau_{\omega,j}^2 \lambda_{\omega,j,t}^2) \quad (6)$$

where $\tau_{\omega,0}$ is the global shrinkage parameter and $\tau_{\omega,j}$ is the shrinkage associated with each predictor variable.

The corresponding evolution log variance equation can be written as

$$\mathbf{h}_t = \boldsymbol{\mu} + (\boldsymbol{\phi}_1 + \boldsymbol{\phi}_2 \mathbf{s}_t)(\mathbf{h}_{t-1} - \boldsymbol{\mu}) + \boldsymbol{\eta}_t. \quad (7)$$

Above, $\mathbf{h}_t = (h_{1,t}, \dots, h_{p,t})$, $\boldsymbol{\phi}_1 = (\phi_{1,1}, \dots, \phi_{p,1})$, $\boldsymbol{\phi}_2 = (\phi_{1,2}, \dots, \phi_{p,2})$, $\boldsymbol{\mu} = (\mu_1, \dots, \mu_p)$, $\mathbf{s}_t = (s_{1,t}, \dots, s_{p,t})$ and $\boldsymbol{\eta}_t = (\eta_{1,t}, \dots, \eta_{p,t})$. Each $s_{i,t}$ for $i = 1, \dots, p$ can be written as follows:

$$s_{i,t} = \begin{cases} 1 & \text{if } \log(\omega_{i,t-D}^2) > \gamma_i \\ 0 & \text{if } \log(\omega_{i,t-D}^2) \leq \gamma_i \end{cases}$$

The idea for ABCO-X is finding a threshold level γ_i for each of the predictor variables and evaluate change points within each varying coefficients $\beta_{i,t}$, separately. For MCMC sampling, each threshold level γ_i will be evaluated conditional on all other threshold levels. Overall, the same sampling scheme is used

for the multivariate case as the univariate case.

6.3 Further Simulation Studies

The Rand index measures similarity between two different segmentations of a series. Let X denote a segmentation given by a model and let Y denote the true segmentation of the series. All pairs of points can then be divided into four groups: pairs that are placed in the same segment in X and in same segment in Y (A); pairs that are placed in same segment in X and in different segments in Y (B); pairs that are placed in different segments in X and in same segment in Y (C); pairs that are placed in different segments in X and in different segments in Y (D). The Rand index is calculated as $\frac{A+D}{A+B+C+D}$. The Adjusted Rand index corrects for the random chance that pairs of points will be placed together. We utilize the Rand index and adjusted Rand index as they give a simple but holistic measure of similarity between the estimated segmentation and the true segmentation.

6.3.1 Multiple Changes in Mean with Heteroskedastic Noise, and varying SNR

Extending upon the simulations in Section 3.1, we generate $N = 100$ series of length $T = 1000$. For each series, the number of change points are generated uniformly at random from the set $\{2, 3, 4\}$. Change point locations are uniformly sampled but with the constraint that their minimal distance is 30 time increments. The resulting segments are each assigned a mean uniformly distributed between -20 and 20 . Finally, innovations with stochastic volatility are added to the mean signals, with log volatility specified as

$$\log(\sigma_{\epsilon,t}^2) = \phi_{\epsilon} \log(\sigma_{\epsilon,t-1}^2) + \alpha_t, \quad \alpha_t \sim N(0, \sigma_{\alpha}^2). \quad (8)$$

For these additional simulations, we consider varied values for ϕ_{ϵ} and σ_{α}^2 to better understand how ABCO and other changepoint algorithms perform across varied signal to noise ratios. We focus on two additional settings: (i) $\phi_{\epsilon} = 0.6$, $\sigma_{\alpha}^2 = 1$; (ii) $\phi_{\epsilon} = 0.9$, $\sigma_{\alpha}^2 = 2$. The results are shown in Table 4.

As shown in Table 4, ABCO has the strongest performance across both settings. In (i) with lower variance and lower auto-correlation ($\phi_{\epsilon} = 0.6$, $\sigma_{\alpha}^2 = 1$), most methods perform significantly better. While ABCO has the best average Rand value and adjusted Rand value, E.Divisive comes within one standard error in both values. However, ABCO has a much lower average distance from predicted changepoint to true changepoint of 0.72 (se 0.58) in comparison to E.Divisive's 17.76 (se 3.13). This illustrates that ABCO identifies many fewer false positives. In (ii) with higher variance and higher auto-correlation ($\phi_{\epsilon} = 0.9$, $\sigma_{\alpha}^2 = 2$), ABCO once again outperforms the rest in terms of all metrics. PELT, WBS and BCP significantly over-predicts number of changepoints here. Despite the higher signal-to-noise ratio, ABCO still maintains a low average distance from the estimated changepoint to a true changepoint of 0.90 (se 0.13), showing the robustness of ABCO even in high noise settings.

Table 4: Results for Changes in Mean with Heteroskedastic Noise, varying SNR

Mean Changes with Stochastic Volatility, $\phi_e = 0.6$, $\sigma_\alpha^2 = 1$

Algorithms	Rand Avg.	Adj. Rand Avg.	Avg. Diff. CP	Avg. Dist. to True
ABCO	0.963 _(0.009)	0.923 _(0.017)	0.32 _(0.06)	0.72 _(0.58)
Horseshoe	0.691 _(0.024)	0.468 _(0.037)	1.93 _(0.10)	0.02 _(0.01)
E.Divisive	0.958 _(0.007)	0.913 _(0.014)	0.77 _(0.11)	17.76 _(3.13)
Pelt	0.795 _(0.011)	0.534 _(0.020)	12.70 _(0.58)	128.91 _(7.85)
WBS	0.639 _(0.015)	0.296 _(0.022)	22.60 _(0.57)	148.21 _(7.33)
BCP	0.895 _(0.013)	0.783 _(0.024)	3.88 _(0.79)	34.91 _(4.79)

Mean Changes with Stochastic Volatility, $\phi_e = 0.9$, $\sigma_\alpha^2 = 2$

Algorithms	Rand Avg.	Adj. Rand Avg.	Avg. Diff. CP	Avg. Dist. to True
ABCO	0.883 _(0.013)	0.762 _(0.025)	1.05 _(0.08)	0.90 _(0.13)
Horseshoe	0.658 _(0.015)	0.349 _(0.022)	1.92 _(0.17)	118.03 _(10.55)
E.Divisive	0.857 _(0.011)	0.682 _(0.020)	4.05 _(0.26)	62.86 _(4.45)
Pelt	0.672 _(0.011)	0.170 _(0.008)	144.44 _(3.23)	138.37 _(6.80)
WBS	0.646 _(0.014)	0.307 _(0.020)	142.69 _(1.70)	138.15 _(6.75)
BCP	0.707 _(0.012)	0.303 _(0.017)	74.72 _(5.50)	93.18 _(4.02)

Rand Avg. measures similarity between the estimated partition and the true partition; the value ranges between 0 and 1, with 1 being a perfect match. Adjusted Rand corrects Rand for the random chance of predicting the correct partition. Avg. Diff. CP. reflects the average difference between true and predicted number of change points. Avg. Dist. to True measures the average distance from an estimated change point to the nearest true change point. The standard error for each measurement is shown in parentheses.

6.3.2 Dynamic Regression Simulation Scenarios

For dynamic regression simulations, the goal is to test ABCO-X's ability to detect changes in the coefficients of the predictors. We simulated 100 series of lengths 100, 200, 400 with Gaussian noise, with variance 1. For each series, we generate three predictors ($\mathbf{x}_t = [x_{1,t}, x_{2,t}, x_{3,t}]$): the first predictor ($\{x_{1,t}\}$) is a vector of 1s; the second predictor ($\{x_{2,t}\}$) and the third predictor ($\{x_{3,t}\}$) are iid standard Gaussian. For the time-varying coefficient matrix $\{\beta_t\}$, the coefficients for the first predictor is piecewise constant, with jumps (two change points) in the middle 50th percentile of the data, while the coefficients for the second and third predictors are random walks with iid increments. The response variable is given as

$$y_t = \mathbf{x}_t' \beta_t + \epsilon_t, \quad \epsilon_t \sim N(0, 1).$$

In this dynamic regression scenario, we only ran ABCO-X on the data as most other change point algorithms are not adaptable to the regression setting. For each simulation, we calculated the average Rand index and adjusted Rand index for each of the three predictors as well as the average number of change points predicted for each predictor. The results are shown in Table 5.

As shown in Table 5, ABCO-X is very accurate for multivariate examples. The algorithm correctly detects change points only in the first coefficient series (predictor 1) while detecting no change points in

Table 5: Multivariate Simulation with Three Predictors

Method	Length (T)	Rand Avg.	Adj. Rand Avg.	Avg. No. CP Pred1	Avg. No. CP Pred2	Avg. No. CP Pred3
ABCO-X	100	0.9966	0.9928	2.34	0	0
	200	0.9932	0.9856	2.44	0	0
	400	0.9846	0.9665	2.67	0	0

Avg. No. CP Pred1 measures on average how many change points are estimated in the coefficient series for predictor 1, and similarly for Pred2 and Pred3. Rand avg. and adjusted Rand Avg. are calculated only for the coefficient of the first predictor.

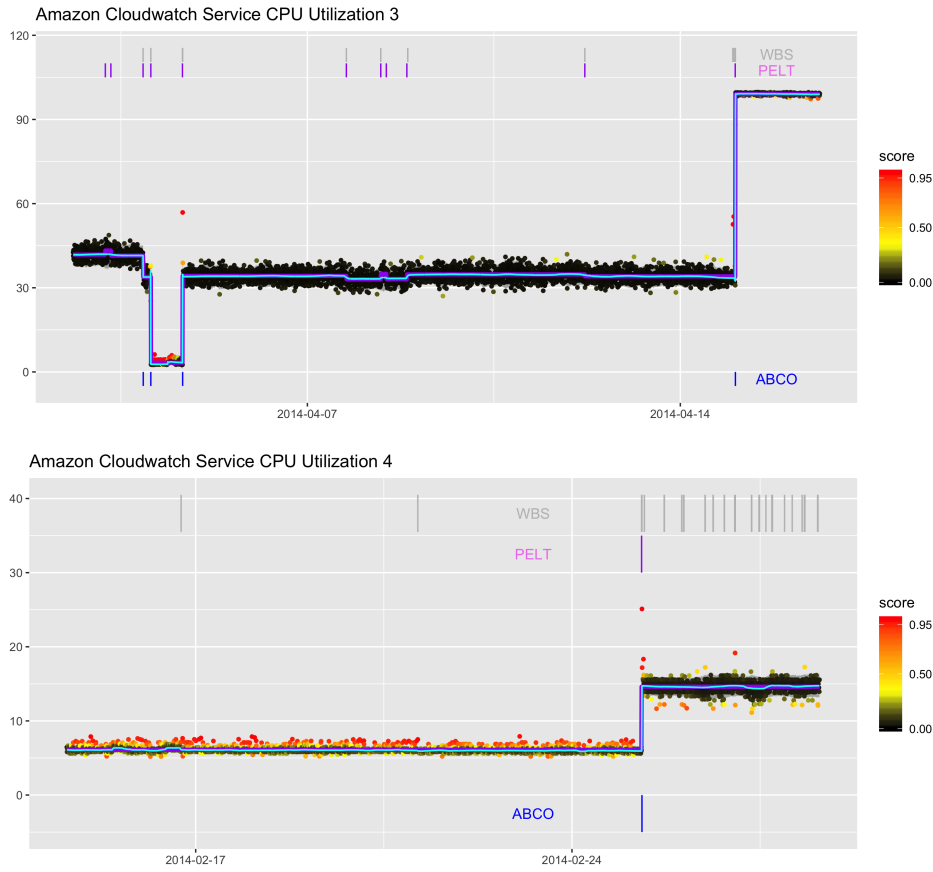
the other coefficient series. The ability to find component specific changes with respect to $\{\beta_t\}$ can be very useful for identifying which predictors most strongly associate with changes in the response variable over time. Across various series lengths, ABCO-X consistently achieves an average adjusted Rand value of above 0.95, showing it can consistently detect the true location of change points even across smaller segments.

6.4 Further Application Examples

6.4.1 Amazon Cloudwatch Server Metrics

Figure 7 illustrates results from running ABCO, PELT and BCP on two additional data of CPU utilization server metrics on Amazon Cloudwatch. Just like in the previous two examples in Section 4.2, ABCO predicts the least number of change points in comparison to PELT and BCP, as ABCO does not chase outliers. As seen in plot for Amazon Cloudwatch Service CPU Utilization 3, ABCO does the best job at not predicting regions with high outliers as change points and not predicting change points at subtle shifts in mean in the middle region of the data.

Figure 7: AWS CPU Utilization Additional Results



Figures show two more examples from applying ABCO, WBS and PELT on additional AWS CPU utilization series. The cyan line represents predicted signal from the ABCO algorithm and purple line represents predicted mean from PELT. Change points from ABCO are shown by blue vertical bars; change points from PELT are shown by purple vertical bars and change points from WBS are shown by gray vertical bars..